

# A Lightweight Self-Supervised Learning Framework for Multivariate Time Series using Hierarchical-JEPA on ECG Data

Siwon Kim

Research Institute of Basic Sciences, Seoul National University, Seoul, Korea

July 2, 2026

## Abstract

Data analysis in the medical domain often encounters scenarios involving a limited target dataset and a large, unannotated dataset with a general distribution. Under such circumstances, self-supervised learning (SSL) methods are highly effective for utilizing large datasets, making them a popular choice for electrocardiogram (ECG) analysis. This work presents the Event Reconstruction Joint-Embedding Predictive Architecture (ER-JEPA), a lightweight SSL framework for multivariate time series, whose name and two-fold hierarchical structure are inspired by the diagnostic approach of cardiologists. At its core, ER-JEPA features: (1) a two-stage structure that constructs representations for each time interval and subsequently processes these representations as a univariate time series, (2) the hierarchical integration of two Joint-Embedding Predictive Architectures (JEPAs), and (3) a Vision Transformer (ViT) backbone. The structural concatenation of two JEPAs categorizes the model as a Hierarchical JEPA (H-JEPA), designed to encode multiple levels of abstract representations for enhanced prediction on complex tasks. This study reports a successful application of H-JEPA to 12-lead ECG data as a multivariate time series alongside an analysis of the sensitivity of hierarchical representation during the pretraining stage. Pre-trained on approximately 180,000 10-second recordings, the model achieves state-of-the-art downstream performance on the ST-MEM benchmark, with rapid computation and minimal resource usage.

## 1 Introduction

While data is the essence of any analysis, from basic to machine learning, the volume of annotated data has never truly scaled to match our computational demand. This led to the advent of self-supervised learning (SSL), utilizing learning based on the inherent structure of data, as seen with invariance-based methods [1, 2, 3] and generative methods [4, 5, 6]. By learning the essence of data through pretraining on large-scale datasets without explicit labels, SSL frameworks achieve a head start on learning a specific task of interest in the downstream fine-tuning step. Hence, SSL has been extensively utilized in domains with high data availability, such as electrocardiogram (ECG) analysis.

The ECG is a recording of the heart’s electrical signals, a non-invasive test measuring voltage from electrodes attached to the skin [7]. Measured from diverse locations, the ECG is a multivariate time series, with 12 channels in modern standards. As one of the most prevalent tests in the clinical field, the ECG yields large-scale datasets within the medical domain. However, as medical data, the ECG requires annotation by professional technicians for precise classification. Furthermore, due to an abundant number of samples from healthy individuals and typical conditions, the general distribution of ECG data is heavily skewed, which requires subtle screening for collecting target data. Utilizing these constraints to its advantage, various studies have explored the application of SSL frameworks for ECG analysis [8, 9, 10, 11, 12].

Recent research involving SSL frameworks often utilizes the transformer architecture [13] to learn general representations of the input data type, as in [14]. Frameworks like the Masked Autoencoder (MAE) [4], which generates masked data, and Joint-Embedding Predictive Architectures (JEPA) [15, 16], which predict embeddings in the representation space, are standard building blocks in recent studies. This trend is also prevalent in ECG analysis; however, unlike prevalent applications in the domains of natural language processing or computer vision, adaptation for ECG has not been optimal because it does not share identical dimensions with either domain. Following implementations from computer vision, structures designed for two-dimensional data are not optimal in terms of resource usage. Some frameworks designed for data types with a sequential order are more efficient in processing multichannel time series, but they do not examine the full potential of each architecture with respect to multichannel processing, since multichannel analysis is often handled during the tokenization process.

In recent trends concerning general representation processing, architectures with hierarchical representations are rising in prominence, particularly regarding world models [17], designing a model capable of making inferences which require both fine and coarse semantic understanding [15]. Incorporating diverse levels of representation is not only crucial for world model learning but is also required for the diagnostic procedure of a cardiologist during ECG analysis.

In this work, we explore the potential of hierarchical representation learning with JEPA on ECG data. Motivated by the approach of cardiologists in ECG analysis, this study introduces the Event Reconstruction Joint-Embedding Predictive Architecture (ER-JEPA), which is a hierarchical JEPA (H-JEPA) featuring a two-stage structure. This structural separation allows each part to focus on a designated analysis, where the first part concentrates on multichannel processing and the latter part is dedicated to temporal analysis. Moreover, the essence of the structure lies in the concept that the channel module encodes multichannel sequences into univariate sequences, and the temporal module processes these encodings as a univariate sequence rather than a multivariate sequential input. By reducing the analysis of multivariate time series into a univariate case, the model gains significant advantages in temporal analysis with respect to efficiency.

Compared to prior studies on the general representation of ECG data using transformer-based SSL frameworks, ER-JEPA achieves computational efficiency without sacrificing multichannel analysis by restricting it to a dedicated module. Another core design choice is the adoption of two separate JEPAs for each part of the model. Due to representation collapse, concatenating two JEPAs is a double-edged design, since both the input and output of the subsequent JEPA are prone to representation collapse, whereas an identical model could typically be trained using a single JEPA only at the end of the encoder.

This report demonstrates the following:

- ER-JEPA succeeds in learning hierarchical representations on ECG data without representation collapse, even with a concatenated JEPA structure which is inherently more susceptible to representation collapse.
- To mitigate variance in model performance across pretraining, we pretrained multiple encoders to assess optimal strategies and hyperparameters for ER-JEPA on ECG data.
- ER-JEPA consistently achieves competitive performance with transformer-based SSL models on ECG datasets. Specifically, it matches state-of-the-art performance on the ST-MEM [8] benchmark using PTB-XL [18] and CPSC2018 [19], and it surpasses state-of-the-art performance on the PTB-XL fine-tuning downstream task with an AUC of 0.936 and 0.943 for multi-label and multi-class evaluation, respectively.
- ER-JEPA presents a highly efficient, lightweight solution among ViT models with multichannel processing, achieving a substantial reduction in both memory usage and inference time.

## 2 Background

In the field of representation learning, self-supervised learning is a framework that is advantageous when an extra unlabeled dataset is available. Without proper labels, SSL methods generate new labels that can be deduced within the inherent structure of the data, e.g., prediction of a hidden part from a given context of the data, or requiring similarity from the invariance of the data. In particular, SSL frameworks targeting a general representation of data with transformer architectures are readily used in recent studies.

### 2.1 Self-Attention and Vision Transformer

Introduced in the celebrated paper “Attention is All you Need” [13], self-attention is a token-wise operation that applies mutual correlation between tokens in an input sequence to produce an output result. Attention was originally designed for natural language processing, but it is now used in various fields, including computer vision. Vision Transformer (ViT) [20] is a transformer architecture tailored for image data which takes patches of a partitioned image as an input sequence. In addition, it uses two-dimensional positional embeddings where a *positional embedding* is a vector that is added to tokens to indicate the order of the tokens within the input sequence. Regardless of the domain, the operation essentially takes discrete tokens as an input; hence, the input data needs to be discretized, such as partitioning an image into patches for image data.

While a self-attention algorithm may be implemented as a broader compound structure, its core mechanism—regardless of further generalizations—consists of the following operation. Given  $N$  tokens  $\{X_i \in \mathbb{R}^{d_{\text{emb}}} \mid 1 \leq i \leq N\}$  with embedding dimension equal to  $d_{\text{emb}}$ , we let  $Q, K, V \in \mathbb{R}^{N \times d_{\text{emb}}}$  be matrices with a linear transformation of tokens  $X_i$  as a row, where the linear transformations of each  $Q, K, V$  are learnable. Written in matrix form, the output is

$$\text{softmax}\left(\frac{QK^\top}{\sqrt{d_{\text{emb}}}}\right)V,$$

where we can figuratively consider each row, a transformation of an input token, as a linear combination of vectors with mutual correlation:

$$\alpha_{i,1}v_1 + \cdots + \alpha_{i,N}v_N \quad 1 \leq i \leq N,$$

where  $q_i, k_i, v_i$  are rows of the  $Q, K, V$  matrices, and the attention weight  $\alpha_{i,j}$  is derived from the scaled dot-product such that  $\alpha_{i,j} \propto \exp(\langle q_i, k_j \rangle / \sqrt{d_{\text{emb}}})$ .

**Notation.** We refer to input tokens within a single attention operation as a *sequence*, and the number of input tokens  $N$  as the *length* of a sequence. With an abuse of notation, we denote the attention operation (possibly with other sub-operations) on tokens  $\{X_i\}$  indexed by  $I$  as

$$\{X_i^{(k)} \mid i \in I\} = \text{AttnBlock}(\{X_i^{(k-1)} \mid i \in I\}), \quad k \in \mathbb{N}$$

for flexible sequence lengths, but losing explicit emphasis on the order of input tokens for the operation. To ease this problem, we interchangeably assume that input patches are already added with positional embeddings that specify the order of the tokens whenever needed.

### 2.2 Image-based Joint-Embedding Predictive Architectures

The Energy-Based Model (EBM) [21] is an SSL framework that learns the correlation between a pair of inputs in terms of energy. The *Joint-Embedding Predictive Architecture* (JEPA) [15] is an EBM framework with two encoders learning their embeddings, followed by a predictor joining the two embeddings. Given a pair of intrinsically linked inputs, JEPA learns the representation

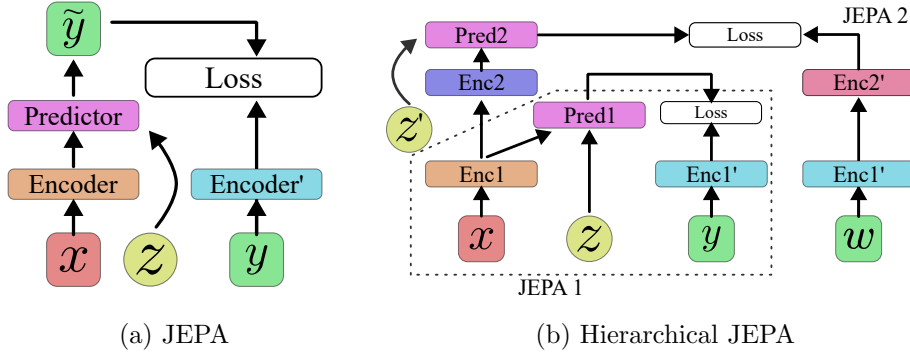


Figure 1: **Overview of Joint-Embedding Predictive Architecture.** (a) The objective of the learning is the prediction of an embedding from a compatible signal with a predictor network, guided by a (possibly latent) variable. (b) Basic example of a two-level Hierarchical JEPA. The latent-space learning process of JEPA is intrinsically suited for hierarchical composition.

of each input by predicting a target embedding from the other embedding and a provided latent variable (see Figure 1a).

The *Image-based Joint-Embedding Predictive Architecture* (I-JEPA) [16] is a JEPA framework on images with a *context* and *target* encoder pair. The architecture learns the representation of image patches by predicting blocks of patches (targets) given a sparse collection of patches (context), in a representation space. In contrast to generative architectures like MAE [4] which learn from reconstructing the raw data form of a target selection from the context, predictions are made in the representation space, and this has been reported as an essence of performance enhancement. Hence, I-JEPA has been widely used in various fields even with data types other than images. And I-JEPA is also a core building block for the proposed architecture.

### 2.3 Hierarchical JEPA

Each encoder in a JEPA is constrained to designated input data specifications with a fixed scope and resolution. For instance, given a pair of an image and text as a single sample, one may assign a target encoder to process the image and the other to process text data. Furthermore, encoders with different tokenization can have distinct resolutions (e.g., varying sampling frequencies) or scopes (due to different patch sizes) for input tokens.

In the literature of representation learning, there are often references to a hierarchy of representations, and in the context of JEPA, *Hierarchical JEPA* (H-JEPA) [15] refers to an architecture with multiple JEPAs with a hierarchy induced from the varying scopes and resolutions of the encoders. Depending on the purpose, one can compose two JEPAs, each processing tokens representing different time intervals (e.g., short and long time intervals) into a single model with an appropriate positional arrangement (see Figure 1b). Researchers theorize that complex tasks need multiple levels of representation, e.g., from coarse representations to finer representations, for an effective understanding of information from the input data.

## 3 Method

Given the provided background, the most concise interpretation of ER-JEPA is simply a concatenation of two ViT-based I-JEPAs with different scopes of data. To elaborate briefly, the first JEPA, which we will refer to as the *channel JEPA*, concentrates on learning inter-channel relationships, processing tokens by groups of concurrent patches from different channels; and the latter, the *temporal JEPA*, focuses on learning intertemporal information between each time

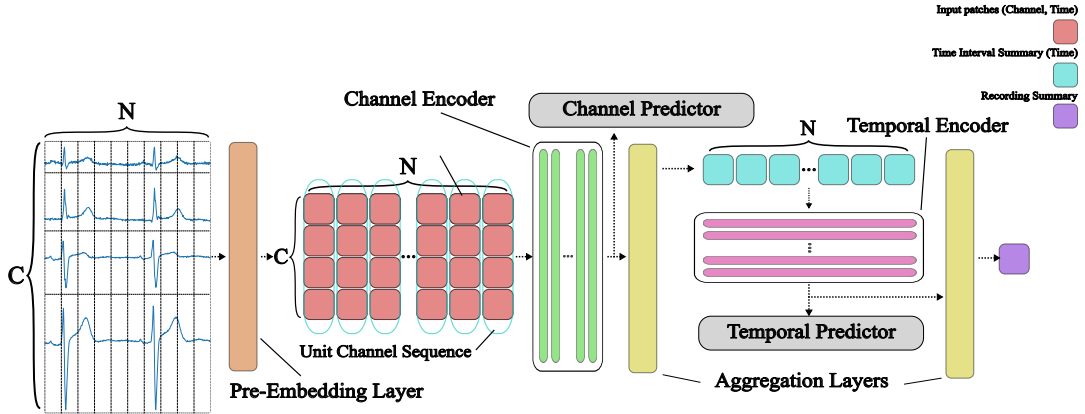


Figure 2: **Schematic of ER-JEPA.** For a multivariate time series with  $C$  channels, the pre-embedding layer first tokenizes the recording into  $C \times N$  patches indexed by (channel, interval). Next, the event reconstruction module, which consists of a channel encoder and an aggregation layer, produces a sequence of tokens representing each time interval. The event analysis module then processes the resulting sequence to capture temporal relationships across tokens. An additional aggregation layer summarizes the interval tokens into a single token, which corresponds to a summary of the entire recording. The depicted predictors indicate their locations as part of the corresponding JEPAs and do not contribute to inference.

interval. By role, the first part of the model (containing the channel JEPA) summarizes each time interval of a multivariate time series into a single representation, and the second part (containing the temporal JEPA) processes representations constructed by the preceding part, focusing on temporal relations. We refer to Figure 2 for the schematic of the model.

Throughout the discussion, we will consider a multivariate time series as a collection of patches where each patch is a vector representing each time interval of some channel, with a natural two-dimensional index (channel, time).

### Problem of Multivariate Time Series with Transformer Frameworks

The two simplest implementations of I-JEPA for multivariate time series both involve modifications of image data handling, adjusted for time series. The first is by treating multichannel time tokens as patches of an image, considering the channel-time index as the 2D coordinates of each image patch. The second is by converting a multivariate time series into a univariate time series during the preprocessing step, e.g., by configuring a single convolutional layer to accept multiple channel inputs in the tokenization step. Each method tokenizes the input sample into 2D or 1D patches, and then the attention layer processes the sequence of patches, where the sequence is a collection of every interval and channel.

These are simple and direct implementations that can be effective, but each is not without its problems. With the first method, every attention layer experiences a factor  $N_{\text{ch}}$  increase in sequence length for a  $N_{\text{ch}}$ -channel time series, compared to the case of a univariate time series. Because the time and memory complexity of the standard attention algorithm is quadratic in the sequence length  $N$ , an increase in sequence length by  $N_{\text{ch}}$  makes quick analysis using transformer models infeasible. On the other hand, multichannel analysis during the preprocessing step may have less impact on complexity since the embedding dimension  $d_{\text{emb}}$  is at most linear in both time and memory complexity. However, since this method handles multichannel analysis before

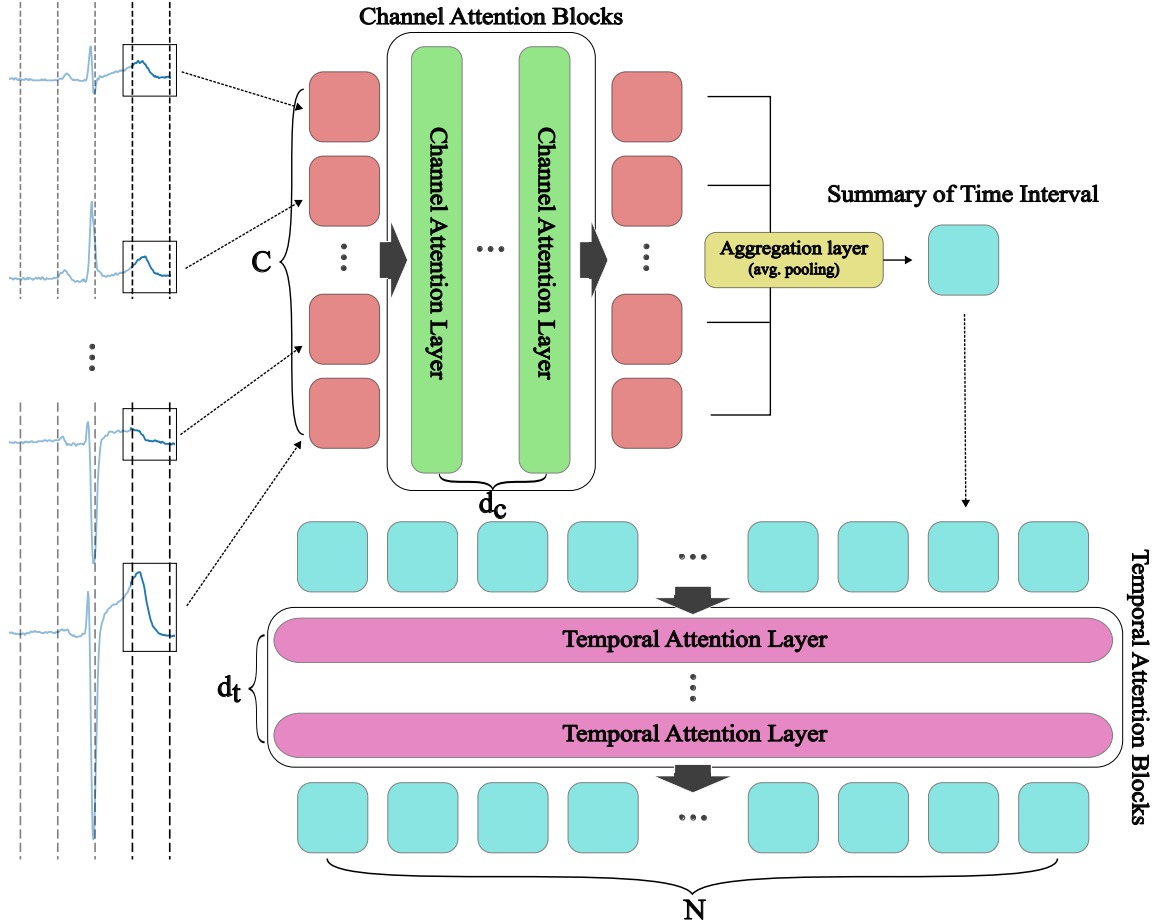


Figure 3: **Forward Pass of Unit Channel Sequence.** Given tokens of a multivariate times series indexed by (channel, time interval), channel attention layers process the input by time interval, taking concurrent tokens of every channel as a unit sequence. Next, an aggregation layer summarizes the  $N_{\text{ch}}$  tokens of each time interval into a single token. These summarized tokens then form the input sequence for the temporal attention layer, with a sequence length equal to the total number of time intervals.

the attention layer, it does not fully utilize the power of attention for the analysis of inter-channel relationships. Fusing multichannel information inside each token deprives the main algorithm of the opportunity to perform inter-channel analysis.

### 3.1 Event Reconstruction

Motivated by the diagnostic approach of cardiologists, ER-JEPA is divided into two parts: 1. *event reconstruction* module, and 2. *event analysis* module. A 12-lead ECG represents the electrical activity of the heart, projected across 12 axes [7]. There may be multiple projections with diverse signals, but importantly, every projection shares the **same origin**. Hence, the essence does not lie in impulses found in a specific channel but in an inference of heart activity made from all projected signals. This observation suggests that rather than analyzing patches from every channel, analyzing the representation of reconstructed heart activity is efficient in a situation where multichannel analysis can be cumbersome. Throughout the section, we refer to Figure 3 as a visual guide to facilitate the understanding of the two-stage token processing.

**Event Representation Construction.** Given patches of a multichannel time series

$$\{X_{ij} \in \mathbb{R}^{d_{\text{emb}}} \mid 1 \leq i \leq N_{\text{ch}}, 1 \leq j \leq N_t\}$$

as an input, the objective of the event reconstruction module is to construct a representation of each time interval:

$$\{Y_j \in \mathbb{R}^{d_{\text{emb}}} \mid 1 \leq j \leq N_t\}.$$

To yield a proper representation of each time interval, the module needs to learn the inter-channel relationships of the given data. The module achieves this by composing a Channel JEPA and an aggregation layer. The channel JEPA is a modified I-JEPA, dedicated to learning inter-channel relations by focusing on mutual correspondence exclusively within concurrent patches of different channels. Details on the channel JEPA are discussed in Section 3.2. Through the encoder of the channel JEPA, input patches turn into a refined representation of the corresponding channel and interval:

$$\{\tilde{X}_{ij}\} = \text{ChEnc}(\{X_{ij}\}).$$

Then, an aggregation layer, such as average pooling, summarizes concurrent representations into a single representation:

$$\{Y_j\} = \text{Agg}_i(\{\tilde{X}_{ij}\}).$$

**Event analysis.** With constructed representations  $\{Y_j\}$ , the input for the event analysis module has been reduced from multichannel patches to single-channel time patches. Hence, the event analysis module simply consists of a modified I-JEPA model for univariate time series. Through the encoder of the temporal JEPA, constructed representations  $\{Y_j\}$  turn into a refined embedding of the corresponding time interval  $\{\tilde{Y}_j\} = \text{TEnc}(\{Y_j\})$ . This transition from a multivariate time series to a univariate time series is the core of its efficiency, reducing the sequence length of the attention layers. For an inference that requires a summary of the entire interval, we again feed the final output to an aggregation layer, e.g., average pooling.

$$Z = \text{Agg}_j(\{\tilde{Y}_j\})$$

### 3.2 H-JEPA with Channel and Temporal JEPA

The Channel JEPA and temporal JEPA are both based on I-JEPA; hence, their core mechanisms are identical: ViT modules with self-attention layers; a context encoders, a target encoder, and a predictor for learning joint-embeddings; and updates of the target encoder via an exponential moving average. For a detailed reference on I-JEPA, refer to [16].

**Channel JEPA** Attention layers inside the channel JEPA take tokens with two-dimensional indices as input and return a processed representation of the patches with the same indexing. However, because the objective of the channel JEPA is to learn inter-channel relations, the self-attention operation is applied differently. Rather than taking all patches of every channel and interval as a single sequence, the channel JEPA takes concurrent patches of different channels as a sequence for the self-attention operation.

$$\{X_{ij}^{(k)}\} = \bigcup_{j=1}^{N_t} \text{AttnBlock}(\{X_{ij}^{(k-1)} \mid 1 \leq i \leq N_{\text{ch}}\})$$

Applying self-attention by each time interval, the model concentrates only on returning a representation that accounts for the correlation between concurrent patches of different channels. This reduces the sequence length from  $N_t \times N_{\text{ch}}$  to  $N_{\text{ch}}$ , passing the factor  $N_t$  to the number of self-attention executions. Accordingly, the context and target for the channel JEPA are each collections of concurrent channel patches; i.e., for a given time interval, the channel JEPA predicts patches of target channels, given patches of context channels.

**Temporal JEPA** As mentioned in an earlier section, the temporal JEPA is a simple modification of I-JEPA to process tokens with a single index, adjusted from the case of images to time series. Hence, it similarly consists of an encoder and predictor with self-attention layers. The only differences are the 1D positional encoding and the input, which is not a token from the raw data, but rather a representation constructed by the channel JEPA module.

$$\{Y_j^{(k)}\} = \text{AttnBlock}(\{Y_j^{(k-1)} \mid 1 \leq j \leq N_t\})$$

Adjusted for univariate time series, the context and target for the temporal JEPA are collections of time intervals. Due to taking a representation as input, it is likely that an identical encoder structure without the channel JEPA is more robust against representation collapse. Experiments demonstrate that a repeated JEPA structure has a higher tendency to experience representation collapse, exhibiting a more severe drop in training loss during the early stages (see Section 5.2 and Figure 5b); however, they also show that once the model recovers from this pronounced collapse, it produces representations that yield enhanced performance in downstream tasks (see Table 8).

### 3.3 Implementation for ECG Data

This section details the implementation of ER-JEPA specifically for ECG data.

#### Twelve Lead ECG as a Multivariate Time Series

In standard clinical practice, a 10-second 12-lead ECG recording comprises eight measured leads (I, II, V1, . . . , V6), while the remaining four leads (III, aVL, aVR, aVF) are analytically derived via standard formulas. Consequently, the implementation design formulated the 12-lead ECG as an eight-channel time series. Henceforth, number of channel is set to  $N_{\text{ch}} = 8$ ; and by fixing 250 Hz sampling rate for 10-second recording, length of time series is set to  $T = 2500$ . Then, with formal representation, input ECG is a matrix  $S \in \mathbb{R}^{8 \times 2500}$  with entry  $s_{ij}$ .

**Tokenization** Due to the structural differences between image data and time series data, the patch embedding step is modified for multivariate time series. Given a multivariate time series  $S \in \mathbb{R}^{N_{\text{ch}} \times T}$  and a fixed patch length  $p$ , a single patch corresponds to the  $j$ -th non-overlapping temporal segment of the  $i$ -th channel, formally denoted as

$$S_{ij} = (s_{ip(j-1)+1}, \dots, s_{ip(j-1)+p}) \in \mathbb{R}^p.$$

Then modified from the case of image, a 1D convolutional layer with both the kernel size and stride set to  $p$ , a single input channel, and an output channel equal to the embedding dimension  $d_{\text{emb}}$ —yields the tokenized patch  $X_{ij}$  from the time interval  $S_{ij}$ .

#### Masking Strategy

Inherited from I-JEPA, the two JEPAs require context and target selections for the pretraining process, which are generally referred to as ‘masks’ in the literature. For each batch, the size of the mask is randomly sampled from a provided range, and for each sample within the batch, the mask is generated according to the corresponding strategy. A choice of the selection method depends on the characteristics of the data and the desired effect on representation learning.

**Channel Mask** Because the pool size for sampling contexts and targets from the 12 leads is small, a simple random selection is typically preferable. However, the 12-lead ECG presents an additional constraint that requires a slight modification. The leads of a 12-lead ECG cover

diverse spatial directions: limb leads (I, II, III, aVL, aVR, aVF) project across vertical directions, and precordial leads (V1, . . . , V6) project across lateral directions [7]. Because only the eight measured leads are utilized in this implementation, uniform random selection would introduce a bias toward the lateral projections. To mitigate this bias, the implementation employs weighted sampling for mask selection. Assigning higher sampling weights to leads I and II effectively compensates for the omitted limb leads, ensuring a balanced selection between the lateral and vertical spatial directions.

**Temporal Mask** Similar to the image domain, target selection is performed in continuous blocks to facilitate semantic representation learning. In this implementation, two context sampling strategies are evaluated: (1) a block context strategy, and (2) a random context strategy. Both strategies sample context patches only after excluding the selected target patches from the available pool. The block strategy aggregates consecutive patches—occasionally fragmented by the excluded target regions—whereas the random strategy uniformly samples individual patches across the remaining sequence. Figure 4 provides visual examples of each scheme. For a performance comparison of the two strategies, refer to Table 3.

## 4 Related Work

Due to the high availability of data, there have been various studies on the general representation of ECG using SSL. The work on Spatio-Temporal Masked Electrocardiogram Modeling (ST-MEM) is one of the earlier works based on the Masked Autoencoder (MAE), which also considered the importance of multichannel token processing, referred to as ‘spatio-temporal patchifying’. The benchmark methodology presented in their work featured downstream classification tasks on PTB-XL [18] and CPSC2018 [19], and it has been widely adopted in SSL analysis of ECG data.

Additionally, several studies have investigated the application of JEPA to ECG data; for instance, the work of Weimann and Conrad [11] explored the data-intensive pretraining of I-JEPA, incorporating several image-to-time modifications specifically for ECG data. By utilizing a convolutional layer to tokenize the 12-lead ECG into 1D patches, the model focuses primarily on processing temporal tokens.

Similarly derived from I-JEPA, ECG-JEPA [12] is another JEPA framework designed for 12-lead ECGs. As with ST-MEM, the design of ECG-JEPA accounts for inter-channel relationships analyzed by attention mechanism. It adopts a structure similar to I-JEPA, processing multichannel tokens indexed by (channel, time); however, it differs by partially restricting mutual influences during the attention operation. The Cross-Pattern Attention layer processes tokens based on the ViT attention layer for image data, but for each patch, it restricts the influence of all other patches except for those in the same channel (horizontal) and concurrent patches in different channels (vertical), forming a cross that intersects at the patch.

Furthermore, the evaluation benchmark of ECG-JEPA follows the methodology of ST-MEM, incorporating its own experimental results for baseline models and details for reproducibility. To facilitate a comprehensive comparison, the evaluation in this study followed the methodology of ECG-JEPA.

## 5 Experiments

### 5.1 Pretraining

The paradigm of two-stage training, which first learns the underlying structure of the data using a large unlabeled dataset, is the essence of SSL. Following the methodology of I-JEPA [16], ER-JEPA predicts the encoding of target patches given context patches during the pretraining

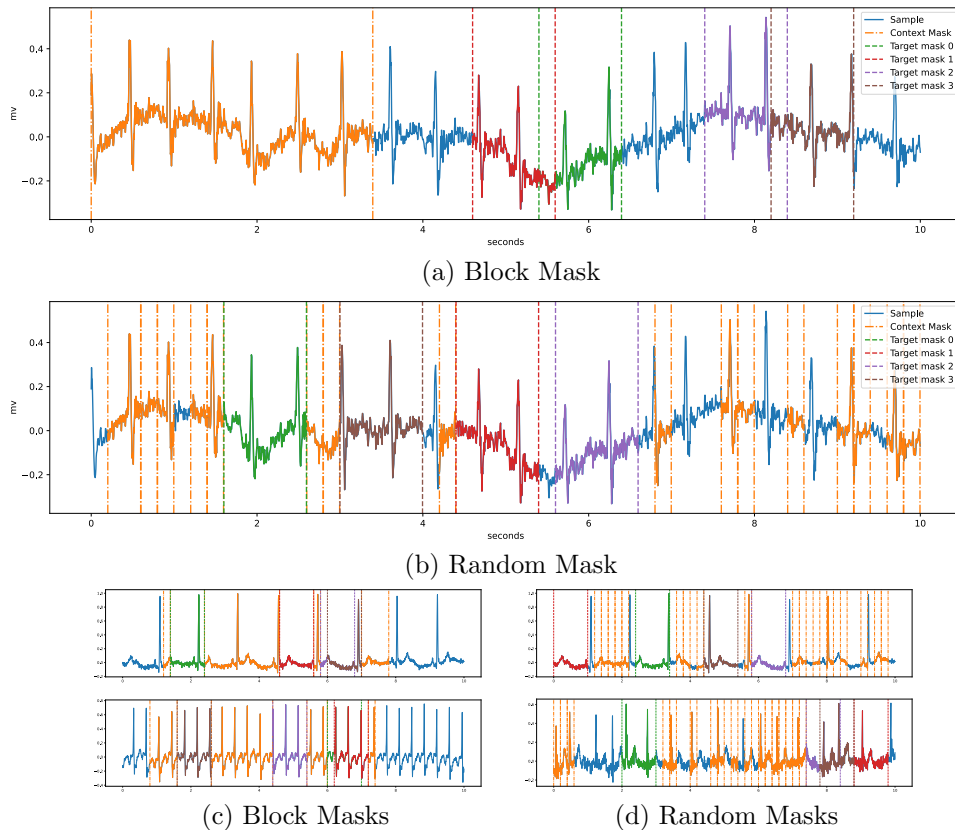


Figure 4: **Example of Temporal Masks.** Context and target masks for each sample are randomly generated based on a predetermined configuration. For each sample within a batch, target masks are sampled as contiguous blocks, with the total target size fixed across the batch. Next, the context mask is sampled from the remaining pool after excluding the target selection; the volume of context selection remains constant across the batch, while the distribution of sampling depends on the chosen scheme. The block mask scheme samples contexts as contiguous blocks (with occasional fragments), the random scheme samples uniformly across the sequence, and the mixed scheme applies the block strategy to half of the batch and the random strategy to the remainder. For each batch, the context mask size is sampled from the range of 1.4–3.6seconds, and the target mask size is sampled from the range of 0.8–1.4seconds.

process. Learning robust semantic representations from the inherent structure of the data requires a large-scale dataset.

### Pretraining Dataset

Due to high data availability, there are various large-scale 12-lead ECG datasets, notably the **Chapman-Shaoxing** dataset [22] comprising 45 152 recordings, and the **CODE-15** dataset [23] comprising 345 779 recordings. Aimed at promoting the analysis of arrhythmias and cardiovascular diseases, the Shaoxing dataset features diverse arrhythmias with labels provided by professional experts, and was collected from Shaoxing People’s Hospital and Ningbo First Hospital. As a subcollection of the comprehensive CODE dataset [24], the CODE-15 dataset represents 15 % of the entire dataset via stratified sampling. Collected by the Telehealth Network of Minas Gerais, this dataset covers a broad patient demographic across Brazil.

**Filtering and Preprocessing** Restricting the scope to 10-second recordings reduces the number of recordings to 143 328 for the CODE-15 dataset. Additionally, recordings containing NaN values or missing leads were removed from the training dataset, yielding a total count of 174 461 recordings, comprising 43 561 from the Shaoxing dataset and 130 900 from the CODE-15 dataset. All recordings were resampled to 250 Hz. No further preprocessing was applied, except for data augmentations added to prevent overfitting across repeated epochs and to enhance the robustness of the learned encodings.

## Training

During pretraining, the model is trained over 300 epochs with a batch size of 64. The AdamW optimizer [25] was used for training, adjusted by a Stochastic Gradient Descent with Warm Restarts (SGDR) scheduler [26], featuring a base learning rate of  $2 \times 10^{-4}$ , a minimum learning rate of  $5 \times 10^{-5}$ , eight restarts, and 10% warmup epochs. The target encoder was updated via an exponential moving average with a linearly increasing momentum value from 0.996 to 1, following the configuration of I-JEPA [16]. Training on a workstation equipped with an NVIDIA GeForce RTX 3090 GPU (24 GB VRAM) takes approximately 30 hours.

## 5.2 Sensitivity of Hierarchical Representation

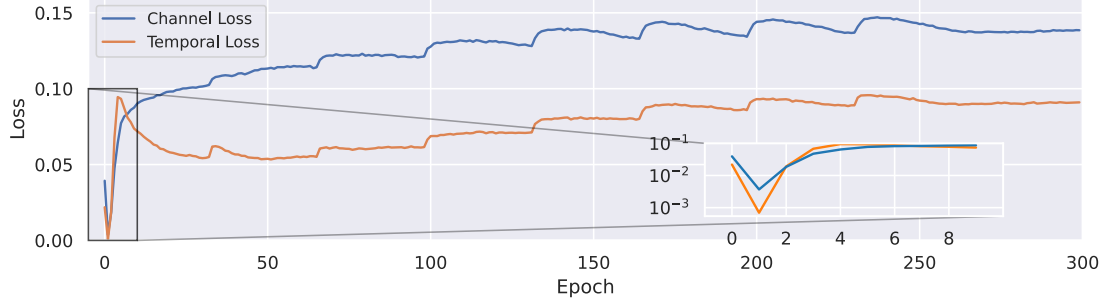
Because the learning process of JEPA operates in the representation space, the architecture is prone to *representation collapse*, a phenomenon where the model trivially solves the prediction task by collapsing all encodings into a constant embedding. This can be largely mitigated by design, such as utilizing asymmetric encoders [27, 28, 2] as seen in many Joint-Embedding Architecture (JEA) models and I-JEPA; however, an inherent susceptibility remains prevalent across joint-embedding architectures.

Representation collapse is an especially serious issue for ER-JEPA, since the input to the temporal JEPA is not a token derived directly from the raw data, but rather a representation constructed by the preceding channel JEPA, which is inherently prone to representation collapse itself. Due to this sensitivity, the performance of ER-JEPA varies significantly with batch size, dataset size, and the embedding dimension. As depicted in Figure 5a, the loss of each JEPA drastically drops in the early stages, then recovers within a few epochs, as is typical for models utilizing the JEPA framework.

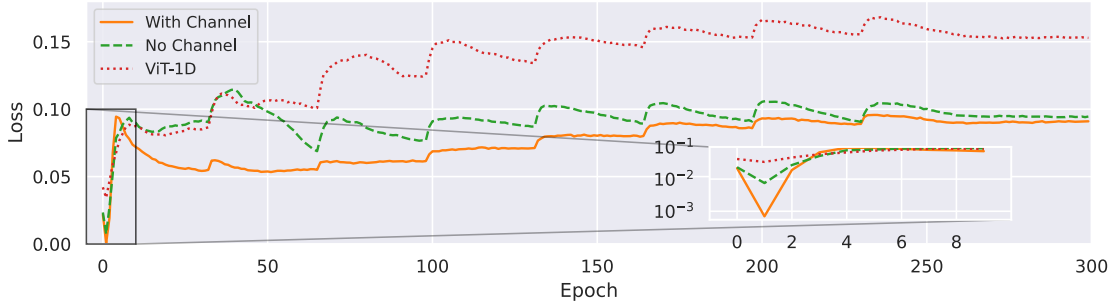
To evaluate this behavior, the evolution of temporal loss can be compared against baseline models without a concatenated JEPA structure, as shown in Figure 5b. Under an identical pretraining environment, both the ablation model without the channel JEPA (detailed below) and the standard 1D I-JEPA adaptation for ECG (see Section 5.3.1) exhibit a visibly less severe drop in loss value during the initial epochs. This distinction highlights that the compound hierarchical stacking in the complete ER-JEPA model amplifies early-stage vulnerability prior to its recovery.

While the complete model ultimately stabilizes, an unrecovered loss during pretraining serves as typical evidence of representation collapse for an experimental model utilizing a JEPA architecture. Building on this observation, the following paragraphs report specific phenomena regarding the sensitive nature of hierarchical representation learning.

**Loss Drop** Because failed attempts at experimental JEPA pretraining often do not recover from an infinitesimal loss in the early stages, a very small loss value is typically considered a harbinger of failure. However, empirical results indicated otherwise for ER-JEPA under specific conditions. With the current pretraining data and a batch size of 64, repeated trials of pretraining occasionally produced anomalous results, yielding inferior downstream performance that significantly deviated from the others (see Table 8). While a definitive explanation remains elusive, the degree of the loss drop for the anomalous trials was **less** severe than in standard



(a)



(b)

Figure 5: **Pretraining Loss of the Channel and Temporal JEPA.** (a) Evolution of channel and temporal loss during pretraining. Both JEPAs exhibit an early-stage drop in loss, with the temporal loss reaching a lower minimum loss of  $7 \times 10^{-4}$ . (b) Impact of the channel JEPA on temporal loss. The plot compares the temporal loss of the complete model against baseline architectures without a concatenated JEPA structure, including an identical model omitting the channel JEPA and a standard 1D I-JEPA adaptation for ECG. The reported loss value is the mean of an element-wise comparison.

trials. To provide a clearer view of this phenomenon, the first two epochs of pretraining were sampled without continuing to the last epoch (see Figure 6). About 1% of the 500 trials exhibited significant deviations in the minimum loss value, for both channel and temporal loss.

**Comparison Without Channel JEPA** An encoder with an identical structure can be trained without the channel JEPA, omitting the predictive process for the channel module. Because the temporal JEPA remains at the end of the encoding layers, the pretraining process remains valid, and the risk of representation collapse is reduced to the level of a single JEPA. Figure 5b compares the temporal loss between the model without the channel JEPA and the complete model. Even under identical training settings, the removal of the channel JEPA prevents the drastic drop in loss during the early stages. However, the absence of the channel JEPA results in noticeable differences in downstream tasks, underperforming compared to the complete model with the channel JEPA (see Table 8).

**Dropout Layer** In conjunction with the hypothesis regarding early-stage loss drops and the predictive nature of pretraining, the performance increase observed from utilizing a dropout layer [29] demonstrates a potential relationship with sensitive representation learning. A dropout layer is an operation activated during the training stage that randomly zeroes out a propor-

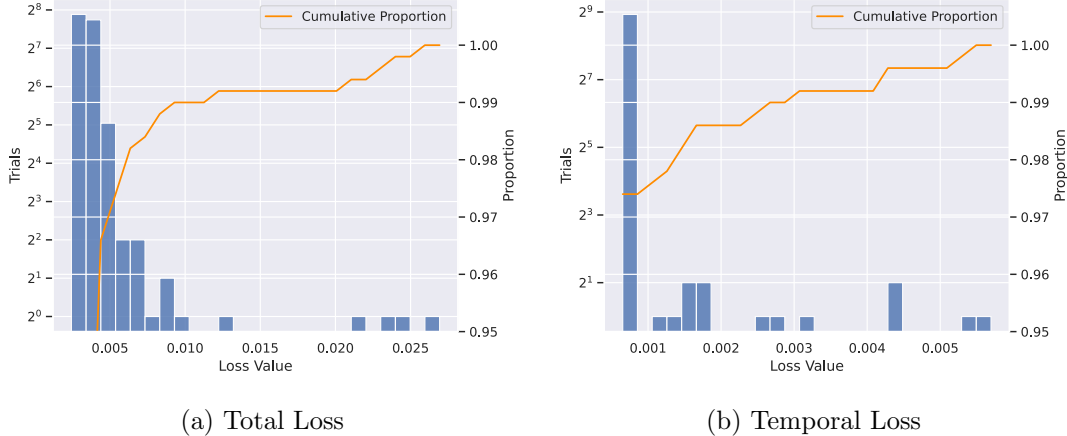


Figure 6: **Histograms of Loss Value at Epoch 2.** Under fixed pretraining configurations, 500 repeated trials yielded approximately 1% of anomalous cases, characterized by relatively high loss values at Epoch 2. This phenomenon was also observed in the rare trials that produced inferior downstream performance. The five trials with the highest total loss corresponded to cases of both channel and temporal loss.

tion of intermediate outputs based on a given probability. As presented in Table 8, the model without a dropout layer exhibits a notable decline in downstream task performance.

### 5.3 Downstream Task

The evaluation of representation learning assesses the encoder’s performance on a specific task, both with and without altering the model. To assess the embeddings produced by the pretrained encoder, **linear probing** evaluates the performance of a basic linear classifier using the frozen encoder’s output as features; for evaluating the full capability of the model, **fine-tuning** trains the entire model end-to-end after appending a classification layer.

The target encoder of JEPA, updated via an exponential moving average, is the standard choice for the **representing encoder** in downstream applications, following I-JEPA [16]. For ER-JEPA, the concatenation of the channel and temporal JEPA encoders, joined by an average pooling layer, serves as the primary encoder for downstream tasks. For the classification of the entire 10-second 12-lead ECG, an additional average pooling layer is appended to summarize the representations of each interval into a single representation (see Figure 2).

#### Downstream Dataset: Classification

Following the benchmarking methodology of ST-MEM [8], the PTB-XL [18] and CPSC2018 [19] datasets were used for the downstream classification tasks. For direct comparison, the macro area under the receiver operating curve (macro AUC) was utilized as the primary metric for all classification tasks.

**PTB-XL** Structured by the Physikalisch-Technische Bundesanstalt (PTB) in Germany, the dataset [18] comprises 21 799 clinical 10-second 12-lead ECG recordings, collected from 18 869 patients. The annotation was performed by two cardiologists, covering 71 different ECG statements conforming to the SCP-ECG standard, which are categorized into diagnostic, form, and rhythm statements. The dataset includes additional metadata for research purposes, such as recommended splits for the training and test sets. Furthermore, the dataset provides two types

of diagnostic labels based on 41 diagnostic statements, aggregated into 24 **subclasses** and 5 coarser **superclasses**.

**CPSC 2018** The China Physiological Signal Challenge (CPSC) 2018 dataset [19] comprises a collection of ECG recordings donated by 11 hospitals for the competition of the same name in 2018. The dataset features eight arrhythmia classes across 6877 12-lead ECG recordings for training and 2954 withheld recordings for testing.

**Labels, Training and Test Set** For PTB-XL, due to its common appearance in multiple works, the superclass was used as the target label for the classification task. Following the provided stratified splits, folds 1 through 8 were used as the training set, while fold 9 (the validation fold) and fold 10 (the test fold) served as the validation and test sets, respectively.

For CPSC2018, all 9 labels, including normal sinus rhythm (healthy individual), were used as target classes. Split by the thousands digit of the record ID, the dataset was divided into 7 batches, with 878 recordings in the final batch. After excluding records with NaN values or missing leads, the first five batches were used as the training set, the sixth as the validation set, and the final batch was used as the test set. The splits for both datasets follow ECG-JEPA [12] to ensure direct comparability.

**Multi-Label and Multi-Class Tasks** Depending on the label structure, the evaluations were further divided into two downstream tasks: multi-label classification and multi-class classification. In the multi-label classification task, multiple labels for a single sample are permitted, without filtering the dataset. Conversely, in the multi-class setting, we filtered out samples with multiple labels, retaining only those with a single label.

### 5.3.1 Benchmark Methodology

Table 1 and Table 2 present the corresponding benchmark results of SSL models on ECG data. The reported scores of SSL models in the original ST-MEM [8] paper are listed as a baseline, along with the test results of the JEPA model from Weimann and Conrad [11], each with possible differences in the splitting of the CPSC2018 dataset. The scores for SimCLR [1], ECG-FM [10], KED [9], and ECG-JEPA are derived from the comparative tests in the work introducing ECG-JEPA [12]. To utilize the extensive evaluation from ECG-JEPA, the assessment of ER-JEPA followed an identical setup for direct comparison.

As a baseline, a simple 1D-JEPA was trained within an identical pretraining environment to ER-JEPA. The structure of this 1D-JEPA follows the framework described in the earlier paragraph of Section 3, where multichannel processing is handled entirely by a convolutional pre-embedding step. This baseline is conceptually identical to the JEPA of Weimann and Conrad, although the specific effects of architectural details may differ. In addition, their JEPA operates on a higher-resolution signal input, with a smaller patch size of 25 and a higher sampling rate of 500 Hz. Furthermore, their study focuses on data-intensive pretraining using 10 public datasets, a larger batch size of 2048, and training epochs on the order of  $10^4$  to  $10^5$ . Hence, considering their data resolution and differences in the pretraining environments, the 1D-JEPA may serve as a surrogate for the JEPA proposed by Weimann and Conrad.

**Downstream Training** The evaluation of models tested in this work followed the procedures outlined below. Because the output of the encoder is merely an encoded embedding, a linear layer, prepended with batch normalization, is appended to serve as the classification head. Taking the representation of the entire recording as input (see Figure 2), the classification layer predicts the diagnostic label for the given sample. Each evaluation process trains the model on the training set, utilizes early stopping based on the validation set, and reports the final

Table 1: **Linear Evaluation Benchmark Results.** Performance (macro AUC) of SSL models on downstream datasets with linear evaluation. Entries with multiple trials are accompanied by standard deviation in parentheses (0.0xx), and the reported value is an average macro AUC over trials.

Model	Pretrain dataset	Records	Multi-Label		Multi-Class		Source
			PTB-XL	CPSC2018	PTB-XL	CPSC2018	
MoCo v3	Shao+CODE15	180 K	-	-	0.739	0.712	[8]
MTAE		180 K	-	-	0.807	0.818	
MLAE		180 K	-	-	0.779	0.794	
ST-MEM	Shao+CODE15	180 K	0.882	0.955	0.879	0.964	[12]
SimCLR		180 K	0.875	0.915	0.830	0.925	
ECG-FM	UHN [10]	622 K	0.878	0.916	0.856	0.931	
KED	MIMIC-IV-ECG	800 K	0.885	0.883	0.888	0.906	
ECG-JEPA	Shao+CODE15	180 K	0.912	0.966	0.903	0.973	
JEPA <sup>1</sup>	10 datasets <sup>3</sup>	1 M	-	-	0.928(03)	-	
JEPA <sup>1</sup>	MIMIC-IV-ECG	800 K	-	-	0.920(02)	0.976(01)	[11]
1D-JEPA <sup>2</sup>	Shao+CODE15	180 K	0.901(01)	0.960(02)	0.888(04)	0.969(02)	This
ER-JEPA	Shao+CODE15	180 K	0.913(01)	0.964(02)	0.911(03)	0.969(04)	
ER-JEPA <sup>1</sup>	Shao+CODE15	180 K	0.913(00)	0.967(01)	0.916(02)	0.973(01)	

<sup>1</sup> 10 trials of downstream training.

<sup>2</sup> Baseline 1D-JEPA model with 5 pretrained encoders.

<sup>3</sup> 1 M recordings sampled from 10 public datasets including CODE15, MIMIC-IV-ECG, and Shaoxing.

evaluation metrics on the test set. Every repeated experiment features a distinctly pretrained encoder, and the number of repetitions is ten for the benchmark comparison and five for ablation studies, unless otherwise specified.

### 5.3.2 Linear Evaluation

The encoder of an SSL model learns embeddings that capture the essence of the data by learning inherent data structures during pretraining. Linear probing evaluates the quality of the embeddings by freezing the encoder of the model and only training the linear classifier appended to the encoder. For details regarding the linear classifier and the evaluation process, refer to the Downstream Training paragraph above. The linear classifier is trained over 70 epochs using a decreasing learning rate starting from  $5 \times 10^{-3}$ , a batch size of 16, and the AdamW optimizer [25].

The experimental results in Table 1 indicate that ER-JEPA demonstrates performance improvements on the PTB-XL dataset, with the sole exception of the JEPA from Weimann and Conrad, which deviates from the performance of the surrogate 1D-JEPA model due to differences in data resolution, architectural details, and pretraining environments. The arrhythmia classification capability of the model on the CPSC2018 dataset is highly competitive with state-of-the-art performance. It is worth noting that the performance differences among baseline models, including ablation studies, are comparatively marginal on the CPSC2018 dataset, where macro AUCs saturate around 0.96; also, for CPSC2018, the splits used to evaluate a few of the benchmark models (from [8] and [11]) are not perfectly identical to the current split (see Section 5.3.1).

As mentioned, the results of linear evaluation primarily assess the quality of the embeddings immediately following pretraining, rather than representing the full capacity of the model. For a complete analysis of the pretraining, refer to the differences in macro AUC between the linear and fine-tuning evaluations in the subsequent Section 5.3.3.

Table 2: **Fine-Tuning Evaluation Benchmark Results.** Performance (macro AUC) of SSL models on downstream datasets with fine-tuning. Entries with multiple trials are accompanied by standard deviation in parentheses (0.0xx), and the reported value is an average macro AUC over trials.

Model	Pretrain dataset	Records	Multi-Label		Multi-Class		Source
			PTB-XL	CPSC2018	PTB-XL	CPSC2018	
MoCo v3	Shao+CODE15	180 K	-	-	0.913	0.967	[8]
MTAE		180 K	-	-	0.910	0.961	
MLAE		180 K	-	-	0.915	0.973	
ST-MEM	Shao+CODE15	180 K	0.929	0.973	0.910	0.977	[12]
SimCLR		180 K	0.918	0.936	0.928	0.955	
ECG-FM	UHN [10]	622 K	0.899	0.922	0.895	0.947	
KED	MIMIC-IV-ECG	800 K	0.901	0.891	0.906	0.923	
ECG-JEPA	Shao+CODE15	180 K	0.931	0.973	0.928	0.976	
JEPA <sup>1</sup>	10 datasets <sup>3</sup>	1 M	-	-	0.935(02)	-	
JEPA <sup>1</sup>	MIMIC-IV-ECG	800 K	-	-	0.928(02)	0.983(00)	
1D-JEPA <sup>2</sup>	Shao+CODE15	180 K	0.923(03)	0.973(02)	0.923(05)	0.979(01)	This
ER-JEPA	Shao+CODE15	180 K	0.936(01)	0.974(01)	0.943(02)	0.981(01)	
ER-JEPA <sup>1</sup>	Shao+CODE15	180 K	0.935(01)	0.973(01)	0.943(03)	0.980(01)	

<sup>1</sup> 10 trials of downstream training.

<sup>2</sup> Baseline 1D-JEPA model with 5 pretrained encoders.

<sup>3</sup> 1 M recordings sampled from 10 public datasets including CODE15, MIMIC-IV-ECG, and Shaoxing.

### 5.3.3 Fine-Tuning

In contrast to linear evaluation, the encoder is trained along with the appended classification layer during the fine-tuning process. For details regarding the linear classifier and the evaluation process, refer to the Downstream Training paragraph above. The entire classification module is trained over 6 epochs using a decreasing learning rate with cosine decay and linear warmup [4] based on  $1.8 \times 10^{-4}$ , a batch size of 16, and the AdamW optimizer [25]. Furthermore, data augmentations, as well as high- and low-pass filtering, are applied, following the training procedures of ST-MEM [8].

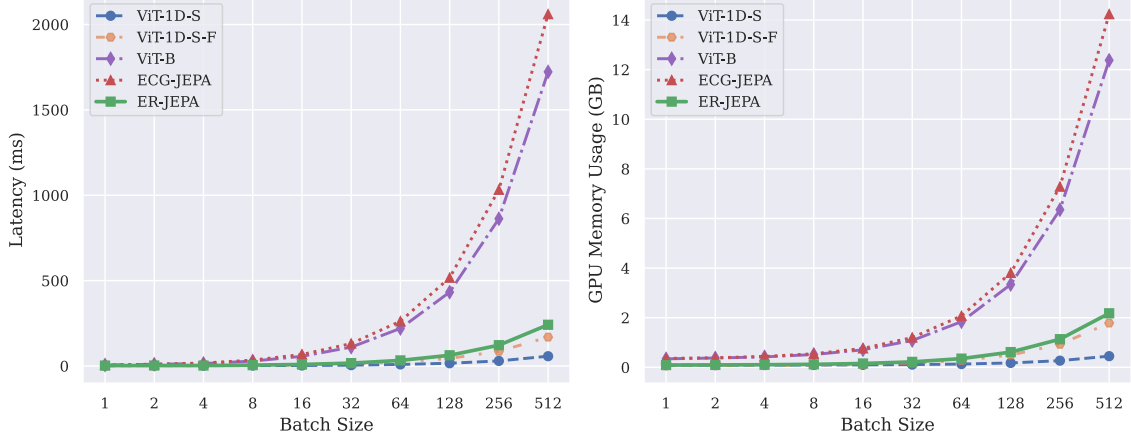
Table 2 presents the benchmark results for the fine-tuning evaluation. As with the linear evaluation, the model excels on the PTB-XL dataset, outperforming the state-of-the-art, and attains state-of-the-art performance for arrhythmia classification on CPSC2018. Again, the performance gap between the model and the 1D-JEPA baseline is comparably narrower on CPSC2018.

Notably, there is a significant increase in the macro AUC scores compared to the linear evaluation, in contrast to the modest 0.007–0.008 AUC increase observed for the JEPA from Weimann and Conrad [11]. The increase observed after fine-tuning suggests that while the pretraining may not inherently force the encoder to learn distinguishing signals for specific tasks, the encoder remains highly adaptable, actively learning new embeddings tailored to the task during the fine-tuning phase.

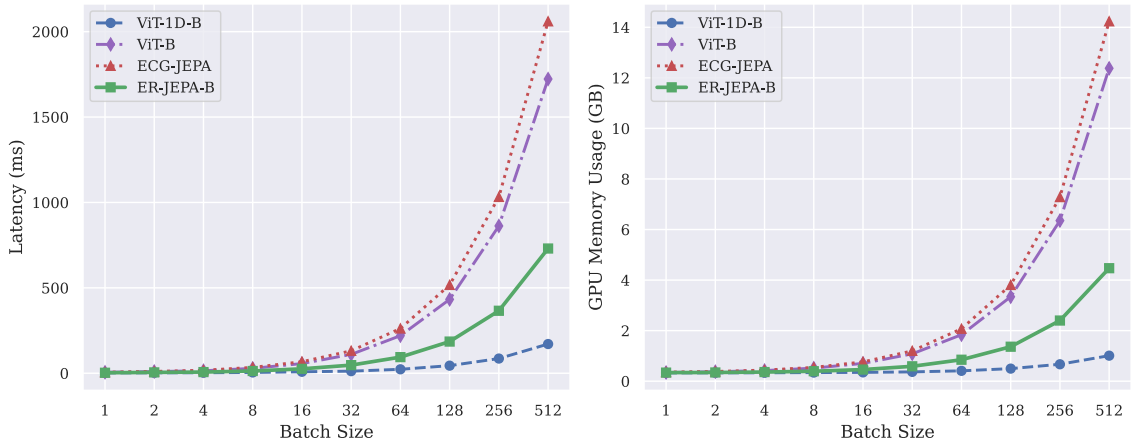
## 5.4 Computational Efficiency

Most ViT-based SSL models in the benchmark results, such as the encoders proposed by Weimann and Conrad [11], ST-MEM [8], and ECG-JEPA, share common hyperparameter standards. Following the configuration of the original ViT [20] or the foundational Transformer [13], an embedding dimension of  $d_{\text{emb}} = 768 (\times 2^i, i \in \{-1, 0, 1\})$  and an encoder depth of 12 are prevalent baseline choices. ER-JEPA in the benchmark also followed this convention, using  $d_{\text{emb}} = 384$ , but splits the network depth, equally distributing six attention layers to the channel encoder and six to the temporal encoder.

While preceding sections 5.3.2, 5.3.3 prove that  $d_{\text{emb}} = 384$  and encoder depths (6, 6) is a



(a) Classification Benchmark Encoders



(b) Encoders under Unified Embedding Dimension

Figure 7: **Computational Efficiency Comparison.** The ViT-based encoders are evaluated based on batch latency and peak GPU memory usage. (a) Performance using the native settings from the downstream classification benchmark. (b) A controlled comparison where all encoders are standardized to a unified embedding dimension of 768.

highly effective configuration, the encoder of ER-JEPA with these hyperparameters gains a significant advantage with respect to resource usage, as half of the attention layers (those in the temporal encoder) exclusively process temporal tokens without requiring multichannel operations. The multichannel processing of the encoder is dedicated entirely to the first module, the channel encoder, which also achieves efficiency through its focused scope. Compared to the temporal encoder, the channel encoder processes a much smaller sequence length of  $N = N_{\text{ch}}$  at the expense of increasing the effective batch size by a factor of  $N_t$ . However, for the current implementation with  $N_{\text{ch}} = 8$  and  $N_t = 50$ , this increase in effective batch size dominates the computational cost over the reduced sequence length, despite the quadratic decrease in attention complexity.

Figure 7 presents an efficiency comparison between ViT encoders of SSL models. The encoder of the ER-JEPA is compared in two settings: (a) under the native settings used in the downstream classification benchmark, and (b) under a unified embedding dimension of  $d_{\text{emb}} = 768$ . The compared models are 1D ViT-S; 2D ViT-B, representing the encoder of ST-MEM; and Cross-Pattern ViT from ECG-JEPA [12]. Furthermore, ViT-1D-S-F, a closer surrogate for the encoder in Weimann and Conrad [11], is additionally compared in the native

setting benchmark to account for differences in data resolution, as their model is designed for 500 Hz data with a smaller patch size of  $p = 25$ . With the hyperparameters used in the classification benchmark, the encoder of ER-JEPA is the fastest among encoders processing multichannel tokens, achieving speeds relatively close to the ViT-1D encoder, which exclusively processes temporal tokens. The encoder achieves up to an  $8\times$  speedup with the hyperparameters used in the classification tasks, and maintains a maximum  $3\times$  speedup even under the unified embedding dimension of  $d_{\text{emb}} = 768$ .

The memory allocation exhibits a similar trend to the speed efficiency. Compared to multichannel ViT encoders in the benchmark, the model requires 70% less memory for small batch sizes and 84% less for larger batch sizes. The larger encoder with an embedding dimension of  $d_{\text{emb}} = 768$  showed similar memory usage for a unit batch size, but baseline encoders consumed two to three times more memory for larger batch sizes.

**Hardware and Software Specifications** The computation benchmark was executed on a workstation equipped with an Intel® Core™ i9-10940X processor and an NVIDIA GeForce RTX 3090 GPU (24 GB VRAM), utilizing Python 3.12.3, PyTorch 2.10.0, and CUDA 12.8 running on Ubuntu 20.04.6 LTS.

**Computation Benchmark Setup** In the experimental script, a random tensor of size  $(B, 8, 2500)$  was used as a single batch of recordings, which was partitioned to a size of  $(B, 8, 50, 50)$  ( $(B, 50, 50)$  for the 1D-JEPA) under a unified patch size of  $p = 50$ . For the additionally compared ViT-1D-S-F model, which operates on a different data resolution, an input tensor of size  $(B, 8, 5000)$  was used with a patch size of  $p = 25$ , yielding an initial patch tensor of size  $(B, 8, 200, 25)$ . The latency per batch is an average over 100 iterations, preceded by a warmup phase of the same number of iterations. After the warmup phase, memory usage was cleared using `torch.cuda.reset_peak_memory_stats`, and both phases were followed by `torch.cuda.synchronize`. For measurement, `time.perf_counter` recorded execution time with high precision. Just-in-Time compilation using `torch.compile` was disabled during the experiment. Each experiment was repeated five times, and the standard deviations reached a maximum of 1% for small batch sizes (under four), while the majority remained well below 1%.

## 6 Ablations

The assessment for the ablation study followed the same procedure outlined in the paragraph in Section 5.3.1. The following sections feature ablation studies evaluating different hyperparameters based on linear and fine-tuning evaluation performance. While each analysis demonstrates that the current hyperparameter configuration is optimal, ablation studies using fine-tuning evaluation exhibit significantly narrower margins, showing stable performance across various ablations.

### 6.1 Linear Evaluation Across Ablations

**Masking Strategy** As discussed in Section 3.3, two masking strategies for the temporal pretraining process are compared in Table 3. To leverage the effects of both masking strategies, a ‘mixed’ scheme was tested, which provides a block mask for half of the batch and a sparse mask for the remainder. Table 3 indicates that while every mask scheme demonstrates strong performance, the block mask scheme outperformed the others on the PTB-XL classification tasks.

**Mask Size** Considering the semantic learning objectives of JEPA pretraining, the size of the context interval is a crucial factor. If the context is too wide, the prediction task becomes

Table 3: **Linear Evaluation Across Masking Strategy.**

Strategy	Multi-Label		Multi-Class	
	PTB-XL	CPSC2018	PTB-XL	CPSC2018
Sparse	0.909(02)	0.962(03)	0.903(05)	0.968(01)
Mix	0.909(02)	0.965(02)	0.903(04)	0.970(03)
Block	0.913(01)	0.964(02)	0.911(03)	0.969(04)

comparatively trivial, whereas a small context may hinder learning due to excessive difficulty. A training strategy utilizing smaller masks sampled from the range of 1.4–2 seconds outperformed the larger mask scheme sampled from the range of 2.8–3.6 seconds. However, the broader range of 1.4–3.6 seconds, which encompasses both ranges, proved optimal by avoiding a fixed trend in size sampling.

Table 4: **Linear Evaluation Across Mask Size.**

Mask Size	Multi-Label		Multi-Class	
	PTB-XL	CPSC2018	PTB-XL	CPSC2018
Large	0.910(01)	0.961(03)	0.903(03)	0.965(03)
Small	0.911(01)	0.963(03)	0.907(04)	0.968(03)
Both	0.913(01)	0.964(02)	0.911(03)	0.969(04)

**Batch Size** For the current pretraining dataset, varying the batch size yielded the linear evaluation performances shown in Table 5. The variation in benchmark performance across these batch sizes is the least significant among all ablation studies. A batch size of 64 is marginally optimal from an overall perspective; however, optimal performance is not guaranteed under different data resolutions, pretraining dataset size, embedding dimensions, or layer compositions. Additionally, the batch size of 64 provided the advantage of offering early indications of failed pretraining, as discussed in Section 5.2.

Table 5: **Linear Evaluation Across Batch Size.**

Batch Size	Multi-Label		Multi-Class	
	PTB-XL	CPSC2018	PTB-XL	CPSC2018
32	0.913(02)	0.962(02)	0.907(03)	0.970(02)
64	0.913(01)	0.964(02)	0.911(03)	0.969(04)
128	0.912(00)	0.964(02)	0.909(03)	0.970(03)

**Time Range for Channel JEPAs Training** Because ER-JEPAs consists of two JEPAs modules, it involves two distinct pretraining processes: one predicting target channels from the context, and the other predicting target time intervals from the given context. Since the pretraining of the channel JEPAs is not restricted by the subsequent temporal pretraining, the range of the time interval used for channel pretraining can be freely selected. Table 6 compares the linear evaluation results of models trained with different time interval selections for channel pretraining. Specifically, a model with the Channel JEPAs pretrained over the context time interval of the temporal pretraining is compared against models pretrained over all time intervals and over the target time interval of the temporal pretraining. The selected time range for channel pretraining may affect the ratio between channel and temporal loss, as well as the overall data scope utilized during the pretraining process.

Table 6: Linear Evaluation Across Training Time Interval

Training Interval	Multi-Label		Multi-Class	
	PTB-XL	CPSC2018	PTB-XL	CPSC2018
Target Mask	0.913(02)	0.966(03)	0.906(01)	0.969(03)
Random Sampling	0.911(03)	0.967(00)	0.907(05)	0.971(03)
All	0.912(01)	0.966(02)	0.908(04)	0.970(05)
Context Mask	0.913(01)	0.964(02)	0.911(03)	0.969(04)

**Embedding Dimension** Similar to the issues discussed regarding the batch size ablation and the sensitivity of hierarchical representation pretraining, a model with an embedding dimension of  $d_{\text{emb}} = 768$  may require a different pretraining environment to achieve optimal performance. However, the ablation study demonstrates that a smaller embedding dimension outperforms the larger model within the current environment.

Table 7: Linear Evaluation by Embedding Dimension.

Embedding Dimension	Multi-Label		Multi-Class	
	PTB-XL	CPSC2018	PTB-XL	CPSC2018
768	0.908(04)	0.951(05)	0.894(04)	0.953(04)
384	0.913(01)	0.964(02)	0.911(03)	0.969(04)

**Without Channel JEPA** As Table 8 indicates, pretraining solely with the temporal JEPA produced a negative effect on representation learning (see Section 5.2). Providing evidence for the necessity of the channel JEPA, this model exhibited inferior performance when compared to the complete model.

**Large Loss and Dropout Layer** Within the current pretraining environment, repeated trials rarely produced significantly underperforming models (see Section 5.2). Table 8 presents the results of models with a loss value at Epoch 2 larger than 0.008. In addition, Table 8 also highlights the performance decrease observed when a dropout layer is omitted.

Table 8: Linear Evaluation Across Miscellaneous Ablations.

Ablations	Multi-Label		Multi-Class	
	PTB-XL	CPSC2018	PTB-XL	CPSC2018
No Dropout	0.908(01)	0.961(06)	0.903(02)	0.969(02)
No Channel	0.902(03)	0.959(06)	0.892(07)	0.965(06)
Large Loss	0.904(03)	0.953(12)	0.900(03)	0.954(10)
Normal	0.913(01)	0.964(02)	0.911(03)	0.969(04)

## 6.2 Fine-Tuning Across Ablations

In contrast to the linear evaluation, the performance of ablation studies on the fine-tuning downstream task did not show significant deviation, although the default hyperparameters remained optimal by a minimal margin. Table 9 presents the average and standard deviation of benchmark results grouped by broader categories. While most of the categories showed saturated performance, the encoders trained without the channel JEPA noticeably deviated from the majority.

Table 9: **Finetuning Performance across Ablation Studies.** The merged categories serve as a superclass of ablation studies: ‘Mask All’ consist of ablations on mask size and strategy; ‘Interval All’, on channel training interval; ‘Batch All’, on batch size other than 64.

Category	Multi-Label		Multi-Class	
	PTB-XL	CPSC2018	PTB-XL	CPSC2018
Large Loss	0.934(00)	0.974(03)	0.943(01)	0.979(02)
No Channel	0.931(01)	0.975(02)	0.936(03)	0.980(01)
No Drop Rate	0.936(01)	0.973(02)	0.941(5)	0.980(01)
$d_{\text{emb}} = 768$	0.935(01)	0.974(01)	0.938(5)	0.978(00)
Mask All	0.935(01)	0.974(01)	0.943(02)	0.980(01)
Interval All	0.936(01)	0.974(01)	0.943(02)	0.980(01)
Batch ALL	0.936(01)	0.975(01)	0.942(03)	0.981(01)
Default	0.936(01)	0.974(01)	0.943(02)	0.981(01)

## 7 Conclusion

This study demonstrates the effectiveness of a lightweight framework utilizing hierarchical joint-representation learning on ECG data. Experiments demonstrate that, contrary to expectations, the concatenation of JEPAs proves robust against representation collapse, and even facilitates enhanced representation learning compared to an identical model with only a single JEPA. By adopting a two-stage structure, where the first module focuses on encoding multichannel inputs into univariate outputs and the second handles temporal analysis, ER-JEPA achieves highly efficient performance with reduced memory usage and rapid computational speed. Through extensive assessment across multiple pretrained encoders, the two-stage structure of ER-JEPA has shown competitive performance in benchmark evaluations, even surpassing state-of-the-art performance on the PTB-XL multi-class downstream task with an AUC of 0.943.

## References

- [1] Ting Chen, Simon Kornblith, Mohammad Norouzi, and Geoffrey Hinton. A simple framework for contrastive learning of visual representations. In *International conference on machine learning*, pages 1597–1607. PmLR, 2020.
- [2] Jean-Bastien Grill, Florian Strub, Florent Altché, Corentin Tallec, Pierre H Richemond, Elena Buchatskaya, Carl Doersch, Bernardo Avila Pires, Zhaohan Daniel Guo, Mohammad Gheshlaghi Azar, et al. Bootstrap your own latent: A new approach to self-supervised learning. *arXiv preprint arXiv:2006.07733*, 2020.
- [3] Kaiming He, Haoqi Fan, Yuxin Wu, Saining Xie, and Ross Girshick. Momentum contrast for unsupervised visual representation learning. In *Proceedings of the IEEE/CVF conference on computer vision and pattern recognition*, pages 9729–9738, 2020.
- [4] Kaiming He, Xinlei Chen, Saining Xie, Yanghao Li, Piotr Dollár, and Ross Girshick. Masked autoencoders are scalable vision learners. *arXiv:2111.06377*, 2021.
- [5] Hangbo Bao, Li Dong, Songhao Piao, and Furu Wei. Beit: Bert pre-training of image transformers. *arXiv preprint arXiv:2106.08254*, 2021.
- [6] Zhenda Xie, Zheng Zhang, Yue Cao, Yutong Lin, Jianmin Bao, Zhuliang Yao, Qi Dai, and Han Hu. Simmim: A simple framework for masked image modeling. In *Proceedings of the IEEE/CVF conference on computer vision and pattern recognition*, pages 9653–9663, 2022.

- [7] Malcolm S Thaler. *The only EKG book you'll ever need*. Lippincott Williams & Wilkins, 2021.
- [8] Yeongyeon Na, Minje Park, Yunwon Tae, and Sunghoon Joo. Guiding masked representation learning to capture spatio-temporal relationship of electrocardiogram. *arXiv preprint arXiv:2402.09450*, 2024.
- [9] Yuanyuan Tian, Zhiyuan Li, Yanrui Jin, Mengxiao Wang, Xiaoyang Wei, Liqun Zhao, Yunqing Liu, Jinlei Liu, and Chengliang Liu. Foundation model of ecg diagnosis: Diagnostics and explanations of any form and rhythm on ecg. *Cell Reports Medicine*, 5(12), 2024.
- [10] Kaden McKeen, Sameer Masood, Augustin Toma, Barry Rubin, and Bo Wang. Ecg-fm: An open electrocardiogram foundation model. *Jamia Open*, 8(5):ooaf122, 2025.
- [11] Kuba Weimann and Tim OF Conrad. Self-supervised pre-training with joint-embedding predictive architecture boosts ecg classification performance. *Computers in Biology and Medicine*, 196:110809, 2025.
- [12] Sehun Kim. Learning general representation of 12-lead electrocardiogram with a joint-embedding predictive architecture. *arXiv preprint arXiv:2410.08559*, 2024.
- [13] Ashish Vaswani, Noam Shazeer, Niki Parmar, Jakob Uszkoreit, Llion Jones, Aidan N Gomez, Lukasz Kaiser, and Illia Polosukhin. Attention is all you need. *Advances in neural information processing systems*, 30, 2017.
- [14] Jacob Devlin, Ming-Wei Chang, Kenton Lee, and Kristina Toutanova. Bert: Pre-training of deep bidirectional transformers for language understanding. In *Proceedings of the 2019 conference of the North American chapter of the association for computational linguistics: human language technologies, volume 1 (long and short papers)*, pages 4171–4186, 2019.
- [15] Yann LeCun et al. A path towards autonomous machine intelligence version 0.9. 2, 2022-06-27. *Open Review*, 62(1):1–62, 2022.
- [16] Mahmoud Assran, Quentin Duval, Ishan Misra, Piotr Bojanowski, Pascal Vincent, Michael Rabbat, Yann LeCun, and Nicolas Ballas. Self-supervised learning from images with a joint-embedding predictive architecture. In *Proceedings of the IEEE/CVF Conference on Computer Vision and Pattern Recognition*, pages 15619–15629, 2023.
- [17] David Ha and Jürgen Schmidhuber. World models. *arXiv preprint arXiv:1803.10122*, 2(3):440, 2018.
- [18] Patrick Wagner, Nils Strodthoff, Ralf-Dieter Boussejot, Dieter Kreiseler, Fatima I Lunze, Wojciech Samek, and Tobias Schaeffter. Ptb-xl, a large publicly available electrocardiography dataset. *Scientific data*, 7(1):154, 2020.
- [19] Feifei Liu, Chengyu Liu, Lina Zhao, Xiangyu Zhang, Xiaoling Wu, Xiaoyan Xu, Yulin Liu, Caiyun Ma, Shoushui Wei, Zhiqiang He, et al. An open access database for evaluating the algorithms of electrocardiogram rhythm and morphology abnormality detection. *Journal of Medical Imaging and Health Informatics*, 8(7):1368–1373, 2018.
- [20] Alexey Dosovitskiy, Lucas Beyer, Alexander Kolesnikov, Dirk Weissenborn, Xiaohua Zhai, Thomas Unterthiner, Mostafa Dehghani, Matthias Minderer, Georg Heigold, Sylvain Gelly, et al. An image is worth 16x16 words: Transformers for image recognition at scale. *arXiv preprint arXiv:2010.11929*, 2020.
- [21] Yann LeCun, Sumit Chopra, Raia Hadsell, M Ranzato, Fufie Huang, et al. A tutorial on energy-based learning. *Predicting structured data*, 1(0), 2006.

- [22] Jianwei Zheng, Hangyuan Guo, and Huimin Chu. A large scale 12-lead electrocardiogram database for arrhythmia study (version 1.0. 0). *PhysioNet 2022* Available online [http://physionet.org/content/ecg\\_arrhythmia10](http://physionet.org/content/ecg_arrhythmia10) 0 accessed on, 23:7, 2022.
- [23] Antônio H Ribeiro, GM Paixao, Emilly M Lima, M Horta Ribeiro, Marcelo M Pinto Filho, Paulo R Gomes, Derick M Oliveira, Wagner Meira Jr, Thömas B Schon, and Antonio Luiz P Ribeiro. Code-15%: A large scale annotated dataset of 12-lead ecgs. *Zenodo*, Jun, 9:10–5281, 2021.
- [24] Antonio Luiz P Ribeiro, Gabriela MM Paixao, Paulo R Gomes, Manoel Horta Ribeiro, Antonio H Ribeiro, Jessica A Canazart, Derick M Oliveira, Milton P Ferreira, Emilly M Lima, Jermana Lopes de Moraes, et al. Tele-electrocardiography and bigdata: the code (clinical outcomes in digital electrocardiography) study. *Journal of electrocardiology*, 57:S75–S78, 2019.
- [25] Ilya Loshchilov and Frank Hutter. Decoupled weight decay regularization. *arXiv preprint arXiv:1711.05101*, 2017.
- [26] Ilya Loshchilov and Frank Hutter. Sgdr: Stochastic gradient descent with warm restarts. *arXiv preprint arXiv:1608.03983*, 2016.
- [27] Alexei Baevski, Wei-Ning Hsu, Qiantong Xu, Arun Babu, Jiatao Gu, and Michael Auli. Data2vec: A general framework for self-supervised learning in speech, vision and language. *arXiv preprint arXiv:2202.03555*, 2022.
- [28] Xinlei Chen and Kaiming He. Exploring simple siamese representation learning. *arXiv preprint arXiv:2011.10566*, 2020.
- [29] Geoffrey E Hinton, Nitish Srivastava, Alex Krizhevsky, Ilya Sutskever, and Ruslan R Salakhutdinov. Improving neural networks by preventing co-adaptation of feature detectors. *arXiv preprint arXiv:1207.0580*, 2012.

## A Hyperparameters

In this appendix, we provide the detailed hyperparameters used for the pretraining, linear evaluation, and fine-tuning phases of the ER-JEPA model.

### A.1 Model Architecture

The ER-JEPA architecture comprises a channel and a temporal module, each with a Vision Transformer (ViT) backbone. Most of the configurations are inherited from widely used baseline configurations, with a slight modification to the number of layers, distributing 12 layers evenly across each encoder. Processing tokens indexed by (channel, interval), the channel JEPA utilizes 2D sinusoidal positional encoding [4]; and processing only temporal tokens, the temporal JEPA utilizes 1D sinusoidal positional encoding [13]. After every attention layer and MLP, a dropout layer with a probability of 0.1 is applied.

Table 10: **Architecture Hyperparameters.**

Hyperparameter	Value
Embedding Dimension ( $d_{\text{emb}}$ )	384
Encoder Depth (Channel & Temporal)	6
Encoder Heads (Channel & Temporal)	12
Predictor Embedding Dimension	192
Predictor Depth (Channel & Temporal)	3
Predictor Heads (Channel & Temporal)	6
MLP Expansion Ratio	$\times 4$
Input Sampling Frequency	250 Hz
Patch Size ( $p$ )	50
Positional Encoding (2D & 1D)	Sinusoidal
Drop Path Rate (Between Layers)	0.1

### A.2 Pretraining

Table 11 summarizes the configurations utilized during the ER-JEPA pretraining phase. Following standard practice, a weight decay of 0.05 was applied exclusively to multidimensional weight parameters, while biases and one-dimensional normalization parameters were excluded from weight decay. Data augmentations, including baseline wander, Gaussian noise, and powerline noise, were applied during pretraining.

### A.3 Downstream Tasks

Table 12 details the hyperparameters used for the downstream linear evaluation and fine-tuning tasks on the PTB-XL and CPSC2018 datasets. The base evaluation procedure follows Section 5.3.1, with extra data augmentations and filtering for the fine-tuning phase as outlined in Section 5.3.3.

Table 11: **Pretraining Hyperparameters.**

<b>Hyperparameter</b>	<b>Value</b>
Epochs	300
Batch Size	64
Optimizer	AdamW
Scheduler	SGDR
Base Learning Rate	$2 \times 10^{-4}$
Minimum Learning Rate	$5 \times 10^{-5}$
Warmup Epochs	10 %
SGDR Restarts	8
Weight Decay	0.05
Target EMA Momentum	0.996 $\rightarrow$ 1.0
Context Mask Size Range	1.4–3.6 s
Target Mask Size Range	0.8–1.4 s
Number of Target Masks	4
Masking Strategy	Block
Channel Time Interval	Temporal Context

Table 12: **Downstream Task Hyperparameters.**

<b>Hyperparameter</b>	<b>Linear Evaluation</b>	<b>Fine-Tuning</b>
Epochs	70	6
Batch Size	16	16
Scheduler	Cosine Decay	Cosine Decay with Warmup
Optimizer	AdamW	AdamW
Base Learning Rate	$5 \times 10^{-3}$	$1.8 \times 10^{-4}$
Minimum Learning Rate	0	0
Weight Decay	0.01	0.05